On the alignment of ZnO nanowires by Langmuir – Blodgett technique for sensing application

[1]Camilla Baratto, [3]Viktoria Golovanova, [2]Guido Faglia, [4]Hanna Hakola, [4]Tapio Niemi [4]Nikolai Tkachenko, [3]Bodgan Nazarchurk, [3]Viacheslav Golovanov

[1]CNR-INO - Via Branze 45, Brescia, Italy

[2]DII, Brescia University, Via Branze 38, Italy

[3]South–Ukrainian National University, Staroportofrankovskaya str. 26, 65020, Odessa, Ukraine

[4] Faculty of Engineering and Natural Sciences, Tampere University, Koereakoulunkatu 7, FIN-33720 Tampere, Finland

Keywords: , Langmuir Blodgett, aligned nanowires, surface reaction, Chemical sensor, ZnO, NO_2, photoactivation.

ABSTRACT

Nanowires are of interest for gas sensing application due to their one dimensional nature and size approaching quantum confinement limit, best studied in single nanowire devices. The reaction between gases and the semiconductor surface is better exploited when one, or few nanowires are involved. Yet, the widespread use of single nanowire devices is prevented by the need of expensive

techniques to fabricate contacts. Here we applied the Langmuir-Blodgett technique to align ZnO nanowires between electrodes being two microns apart in a configuration that possess both the quality of single nanowire devices and the advantages of multiple nanowires. We achieved alignment without using lithography, so the procedure is inexpensive and scalable. As a proof of concept, we demonstrated that the obtained chips are suitable for sensing of NO_2, either at 200°C or at room temperature with light activation. We discussed the obtained sensing parameters as a function of supra and sub-bandgap photoactivation.

1. Introduction

The need for reliable, quick-acting, low-cost detectors for different dangerous chemical agents is evident, and many sensors have been proposed [1,2,3,4]. Such sensors, especially if they are small and consume only a small amount of power, would be far more practical for widespread use than complex and costly analytical instruments.

In order to increase sensor performance, sensors based on individual nanowires (NWs) are highly desirable. Due to almost monocrystalline perfection and atomically sharp terminations, nanowires exhibit excellent chemical and thermal stability that make them superior to conventionally used polycrystalline thin-film sensors, which are often associated with grain coalescence stimulated by high temperature and consequent high drift of electrical properties [5,6,7]. Another advantage of NWs in sensor applications is the small diameter approaching electron confinement limit, which make conductivity of NW extremely sensitive to all changes its surface.

Although devices based on single nanowire have numerous potential benefits in molecular sensor applications [8, 9], there are many practical obstacles in the fabrication of these devices, such as cost, reproducibility, and scalability, to mention just a few. In particular, to fabricate

contacts on individual nanowires is a demanding procedure [10,11] that makes their widespread applications almost impossible.

The conventional approach to the problem goes by finding an effective method of depositing an aligned array of NWs on a substrate which either has pre-patterned electrodes oriented perpendicular to the NW alignment direction or electrodes deposited on top of aligned NWs [12, 13, 14]. This approach does not guarantee the fabrication of devices with single NW bridging the electrodes but comes close by enabling devices with only a few NWs between the electrodes. There are many existing methods of depositing aligned arrays of NW with array thickness limited or close to single NW, e.g., electrospinning [15], microfluidic flow [16], electric field [17], and Langmuir-Blodgett (LB) [18]. The LB method has an advantage of being inexpensive, not requiring special surface pre-patterning, and resulting in a reasonably high degree of alignment of one NW thick arrays [19,20]. **Change C.01** To be suitable for the LB deposition method, the NWs must be hydrophobic or made it by capping with a suitable surfactant. Hydrophobicity keeps them floating on the water surface of the deposition trough. Initially, the NWs are spread on the surface at sufficiently low density and do not touch each other. Surface compression by two parallel barriers forces the NWs to arrange themselves parallel to the barrier due to their large aspect ratio [20]. Such an aligned array of NW is easily transferred on a solid substrate. The method was effective in depositing different types of NWs such as silver [5], tungsten oxide [1], and vanadium dioxide [21].

The present work aims to achieve the deposition of oriented ZnO NWs arrays across the electrodes by employing a Langmuir-Blodgett technique. The arrays of parallel-aligned nanowires possess features and superiorities of a single nanowire, but facilitate the overall manipulation and avoid difficulties in fabrication of reliable electrical nanocontacts. The highly ordered sensors

array minimizes issues arising from the intrinsically random nature of the nanowire network and guarantees higher reproducibility and industrial scalability of the products. As a proof of concept demonstration, we studied the ZnO nanowires aligned between contacts as gas sensors. The tests performed in the present work with reducing (H_2S) and oxidizing (NO_2) species, showed high surface sensitivity to NO_2. Further insights on the surface reactivity was studied by varying the sensing parameters as operating temperature and wavelength for photoactivation.

2. Materials and methods

2.1. Nanowire alignment

We used commercial ZnO NWs from PlasmaChem GmbH, which have a suitable average length (~5 μm) and diameter (50-300 nm) and are available in sufficient amounts for Langmuir-Blodgett procedure: roughly 10 mg of stock NWs was consumed for each experiment. The procedure developed here applies to any NWs produced by different techniques, provided that a sufficient amount is available. Langmuir-Blodgett system used in this work had a small trough (364×75 mm) and allowed constant measurement of the surface pressure with the barriers compression. We adapted the dipping system in such a way that one effortlessly can transfer the films to a horizontal substrate (Langmuir-Schaefer technique).

Commercially available NWs were very inhomogeneous in sizes and contained a large number of agglomerates. Therefore, the first step in sample preparation was the separation of single NWs, achieved by (1) suspending NW powder in isopropanol, (2) sonication, (3) gravity separation, and (4) collection of non-precipitated part of the NW suspension. We repeated the procedure a few times.

Substrates with gold electrodes had 1×1 cm size and contained 7 electrode pairs with an inter-electrode gap of 2 μm and overlap length of 10 μm, see Figure S1 in SI: we tested different configurations of electrodes. The gap between the electrodes was narrow enough so that nanowires could bridge the gap.

2.2. Nanowire hydrophobization and sample purification

To be suitable for alignment and deposition by the Langmuir-Blodgett (LB) technique, the NWs must be hydrophobic. Since metal oxide NWs are generally hydrophilic, the ZnO NWs were coated by palmitic acid molecules, which self-assemble on the surface of ZnO due to their carboxylic groups and expose alkyl tails to the outer side of the layer. We added 1.5 ml of palmitic acid solution in isopropanol (0.1 mg/ml) to a suspension of 10 mg ZnO NWs in isopropanol and sonicated for 10 min in the sonication bath. To remove unreacted palmitic acid, we centrifuged the sample, collected the precipitated, and suspended it in isopropanol again, repeating the procedure fifteen times. Finally, we replaced the isopropanol with chloroform to make the suspension suitable for the Langmuir layer formation.

We spread the obtained suspension of ZnO NWs in chloroform on the water surface of the Langmuir trough recording the surface pressure-area isotherm (see Figure S2 in SI). We deposited the LB films at different target pressures: 10, 15, 18, and 22 mN/m. There was no visible difference between these samples, except that at higher pressure the density of wires was higher, and the wires were slightly more aligned. Figure 1a sketches a schematic presentation of the NW alignment process.

Aligned nanowires were used for sensing tests. For the sake of comparison, dropcast samples consisting of ZnO random nanowires were prepared as well for comparison, by simply dropping NWs dispersed in a solvent over the electrodes (see Figure S3 –SI).

2.3. SEM microscopy

Zeiss Sigma Field Emission Scanning Electron Microscope (FE-SEM) was used to study the morphology of the samples as well as imaging of their conductivity. The low acceleration voltage of 1 kV allowed collecting more information from the surface layers of ZnO nanowires, such as charging.

2.4. Sensing tests

We carried out sensing tests in a stainless-steel test chamber (1000 cm^3) equipped with a quartz window for front illumination, and with an integrated heater holder to accommodate the chip. We kept a constant flux (300 cm^3/min) with 30% relative humidity (RH), diluting gas species (NO_2 and H_2S) from certified bottles. A constant voltage equal to 3V was supplied to the sensing film, measuring the electrical current by a picoammeter (Keithley model 486).

For photoexcitation, we used a He-Cd laser (325 nm and 442 nm lines) and neutral density filters. The light intensity at the sample was 0.5 and 8 mW, respectively.

As a performance feature, we selected the *Relative Response* (*RR*), i.e. the relative change of resistance towards gases $RR = (R_F-R_0)/R_0$, where R_F is the steady state value of resistance in gas, and R_0 is the steady state value of resistance in air. *Response* (*Recovery*) *time* was the interval needed to reach 90% of steady state value in gas (70% of recover to air). Due to the physical

constraint of the test chamber, a complete exchange of the chamber atmosphere takes more than three minutes, so shorter response and recovery times are meaningless in our experimental setup.

3. Results and discussion

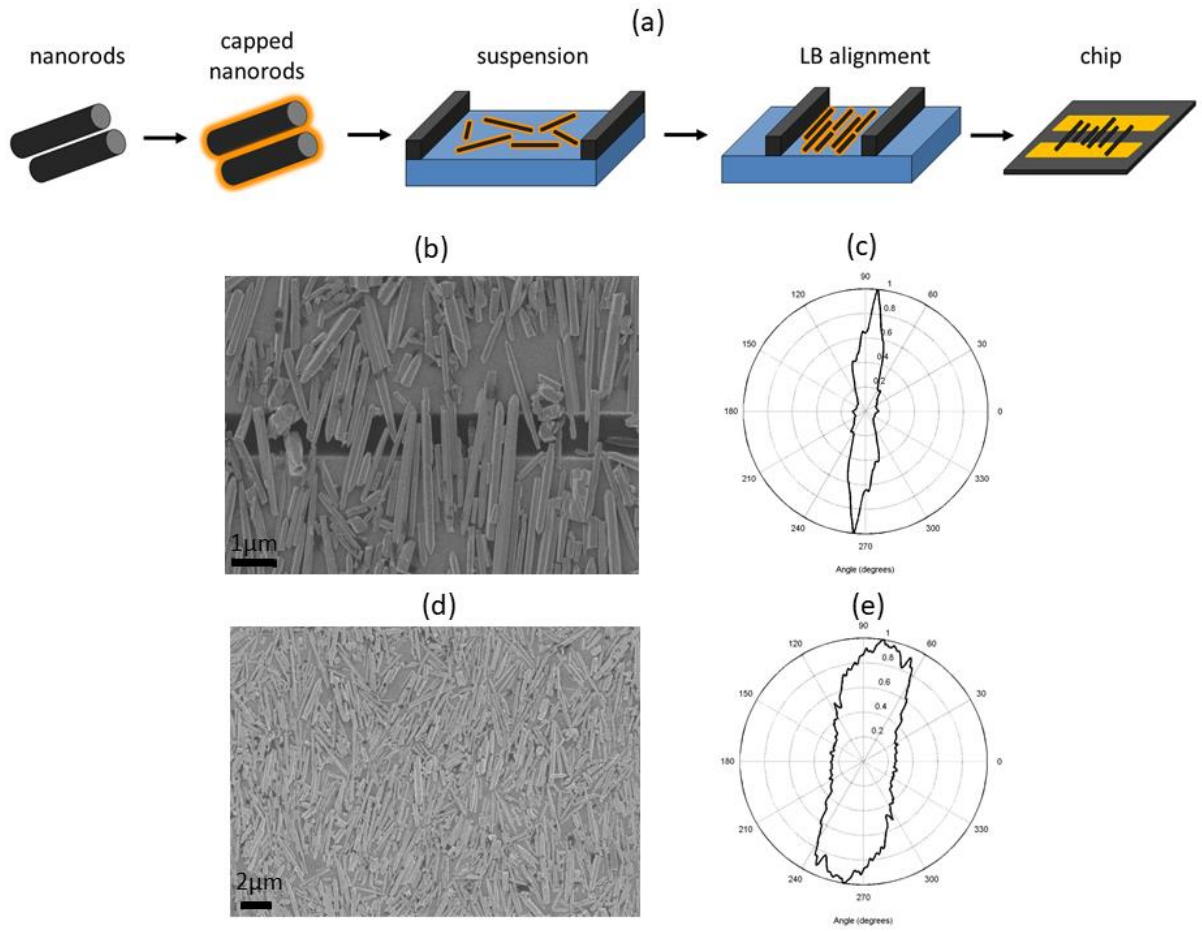

Figure 1: (a) Scheme of the LB alignment procedure (b, d) SEM images of ZnO NW LB films deposited on the Si/SiO_2/Au substrates obtained at different magnification; (c, e) orientation diagrams corresponding to figure (b, d) obtained from SEM images with CytoSpectre software.

SEM microscopy was used to analyze the alignment process. Figure 1(b) shows SEM images of layers deposited on a silicon substrate with Au electrodes: predominant orientation of the NWs takes place, but also a broad distribution of NW sizes results in strong distortion of the order at a larger scale - see Figure 1(d). The orientation factor was studied by analyzing SEM images with CytoSpectre software [22]. Figure 1(c, e) show the corresponding orientation diagrams: typical orientation factors (the ratio distribution value along the orientation axis to perpendicular direction) were 3-5. **Change C.02** This relatively low degree of orientation is most probably due to the broad size distribution of the NWs used, and to the small NW fragments with minimal aspect ratio, that remains after centrifugation. Perhaps a more thorough redispersion-centrifugation could eliminate better undesired small fragments; we did not study this option as achieved orientation factor was sufficient for obtaining a few NW bridging the electrodes.

The reproducibility of obtained monolayers was estimated to be 80%.

Through the LB alignment procedure we were able to almost routinely produce ZnO nanowire samples on gold electrodes for further characterization. Still, the high variation in ZnO nanowire length and thickness of stock samples limits the degree of alignment.

The employed technique leads to a dense film of nanowires covering electrodes and the surrounding area. Percolations between the nanowires arranged around the electrodes may potentially result in occurring of bypasses to the current through the nanowires that directly bridge the electrode gap. In order to eliminate the undesirable additional conductive channels, we have tested different electrode configurations combined with contrast imaging method described by Chung et al. [23]. The approach allowed us to visualize conductive pathways through the percolated

nanowires, which have a higher potential to emit secondary electrons than those contacted only with the dielectric substrate. Figure 2(b) presents the electrodes we have chosen.

Prior to sample conductivity and sensor applicability studies, the samples underwent annealing at 400°C for 30 min. Annealing improves the contact between the NWs and gold electrodes, but more importantly, removes palmitic acid from the NW surface.

Figure 2: SEM images of the ZnO NW LB films with pathways around the electrodes (a) and with no visible bypasses (b).

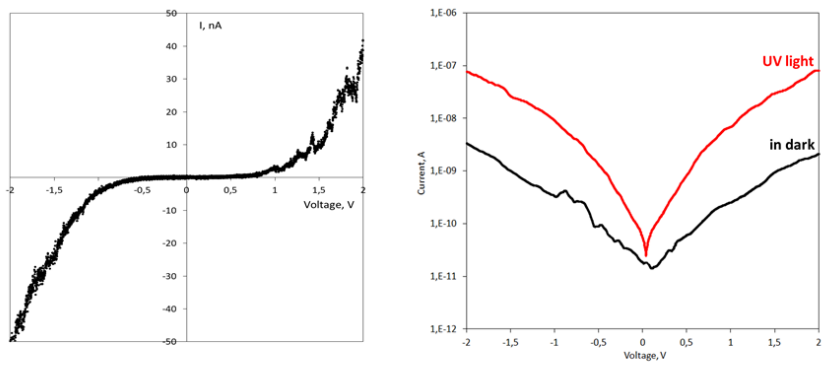

Figure 3: (a) Typical I-V curve of ZnO NWs between Au electrodes; (b) I-V curves in a log scale in dark conditions and under UV light illumination.

Figure 3(a) presents the typical I-V curve of ZnO NW array, showing a rather symmetric response for positive and negative potentials, which indicates a reliable contact between NWs and Au electrodes. The applied voltage ranging between -2 and 2 V proved the stability of the samples, even in a high bias range. As from Figure 3 (b), the current is increased by almost two orders of magnitude under UV light illumination compared to dark conditions at room temperature (RT), due to band to band carrier generation.

Photoelectrical characterization

For electrical characterization, we used light and temperature activation together and separately. Figure 4 (a) presents results of measurements at 200°C together with blue light activation (442 nm - 8mW), Figure 4 (b) show results for the device measured at RT with blue light, and Figure 4 (c) the device measured at RT under UV excitation (325 nm - 0.5 mW). The blue laser does not possess the energy needed to excite band to band transitions but may act on intra-band gap states. UV light generates electron-hole pairs and is common in gas sensing experiments with metal oxides [24].

Figure 4 (a) shows that the current rises instantly when blue light is switched on. When the laser shutter closes, the current rapidly drops down, as can be observed at the arrow, and then increases backward when the blue light is again impinging on the sample. It takes a few minutes after switching on the light to reach a steady state current, while the current decreased in a few minutes when the laser is switched off. Figure 4 (b) shows the effect of laser light on the sample kept at RT (25°C). The current reaches a steady state after about ten minutes. The steady state value is 9×10^{-9} A, slightly lower than the current observed in Figure 4 (a), which is 3×10^{-8} A; the small difference is ascribable to the temperature activated carriers. The other difference is the noise observed at

elevated temperature (200°C) compared to other cases: thermally activated carriers inside the nanowires may explain the noise [25] since it disappears in measurements at RT.

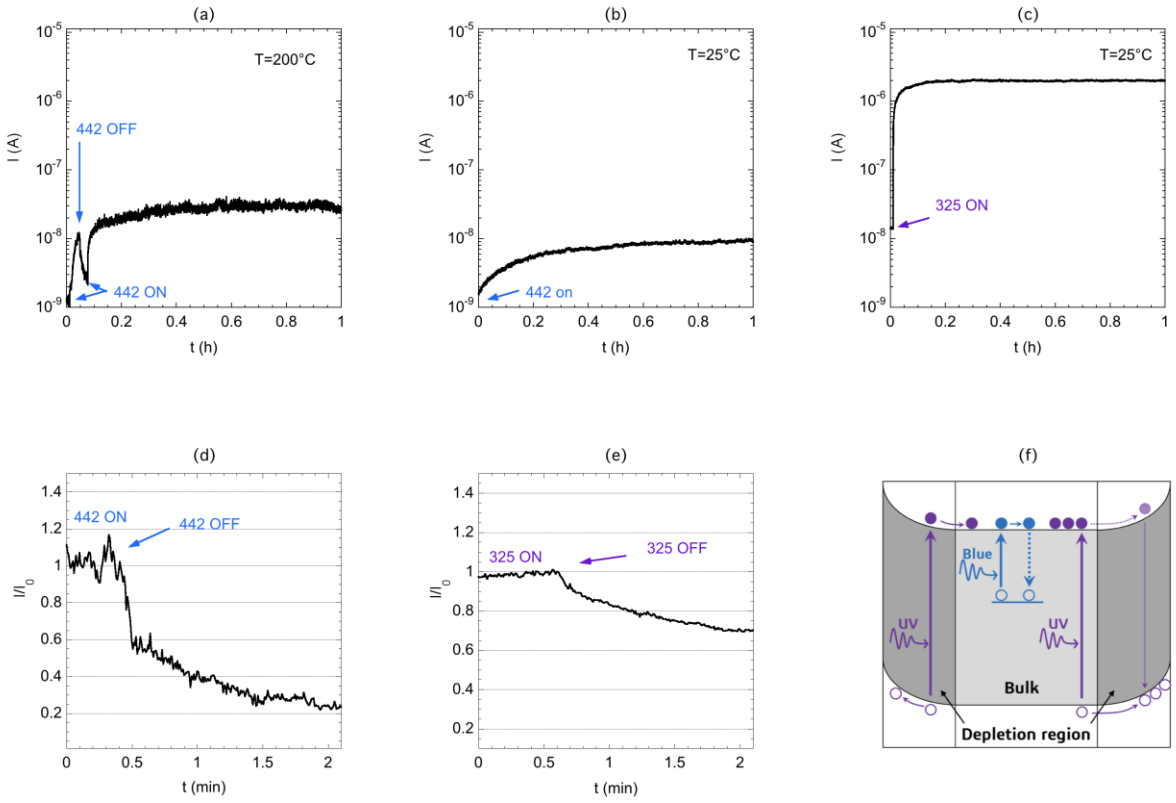

Figure 4: Current flowing through the sample exposed to humid air at 30% RH in different conditions: (a) working temperature 200°C; blue laser was switched on at t=0 and shuttered at t=4 minutes for 2 minutes to check light influence; (b) RT operation: blue laser was switched on at t=0; (c) RT operation: UV laser was switched on at t=0; (d) current decay after switching off the blue laser light at 200°C; (e) current decay after switching off the UV laser light at RT; (f) scheme of the photoactivation process.

Figure 4 (c) shows the effect of illumination with UV light. The current at *t*=0 was the one obtained with blue illumination. Electron - hole pairs generated by UV light promote a two order

of magnitude increase of the current, comparing to dark conditions at RT. **Change C.03** The time needed to reach the steady state further decreased to 2.4 minutes compared to the illumination with blue light.

Photogenerated holes recombine with oxygen ionosorbed at the surface of ZnO, thus decreasing the space charge layer thickness at the surface of the nanowire and increasing the current flowing through the nanowire. The transient time value is in agreement with what is reported in literature for UV light induced oxygen photodesorption in SnO_2 [26, 27, 28].

After switching off the blue laser, the photoconductivity drops down promptly (Figure 4 (d)); however, when the UV illumination goes off, the photocurrent decays slowly, as shown in Figure 4 (e). Apparently, under the UV band-to-band excitation, the electrons accumulate in the bulk of the nanowire, while the photogenerated holes drifted to the surface due to the band bending caused by chemisorbed oxygen species. The emerging charge separation leads to the increased lifetime of the photogenerated carriers. Thus, slow descent of the current observed after turning off the UV excitation can be governed by a hindered recombination of the spatially separated non-equilibrium carriers through the surface barrier. By contrast, blue laser excites electrons from the trapping centers not deeper than 2.8 eV from the conduction band minimum, and their recombination lifetime will strongly depend on the localization of the defects. As the photocurrent quickly decays down, we suggest that these trapping centers mainly originate not from the surface but rather from the bulk, as depicted in the scheme of the photoactivation (Figure 4 (f)).

We investigated the sensing performance of the device towards NO_2 at a constant relative humidity under different types of activation (Figure 5): temperature at 200°C + light at 442 nm, RT + light at 442 nm, and RT + light at 325 nm. Figure 5 represents the sensitivity tests to NO_2 for different working conditions. Table 1 report the data obtained from measurements depicted in

Figure 5. The relative response of the sensor is the same, but the noise observed when operated at 200°C is much higher than when operated at RT and excited both with 442 nm and with 325 nm laser light. Response and recovery times are shorter for light at 325 nm while they are longer for at 442 nm and RT.

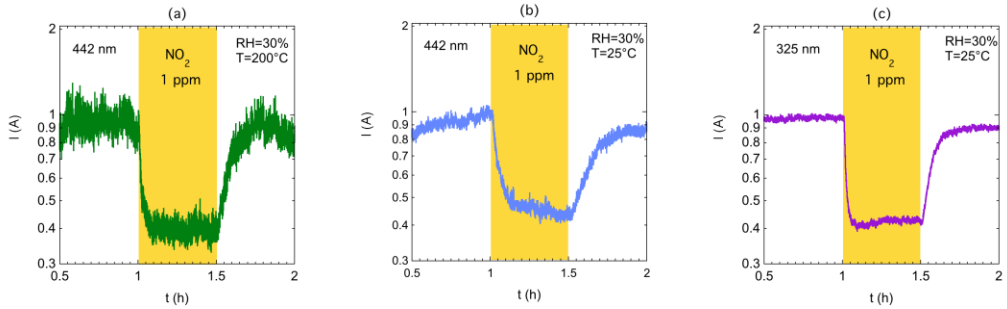

Figure 5: Sensing NO_2 (1 ppm) with aligned nanowires in different conditions: (a) 442 nm and temperature activation (T=200°C); (b) 442 nm activation at RT (c): 325 nm activation at RT.

Table 1: parameters extracted from measurements in Figure 5**.**

	Relative response	Baseline noise (variance)	Response time (min)	Recovery time (min)
442 nm -200°C	1.44	0.006	3	11
442 nm - RT	1.29	0.002	10	23
325 nm - RT	1.38	0.0001	3	13

Since the measurements of the samples heated at 200°C were too noisy, and while the ones using blue light excitation were worse than those with UV light, we chose to carry out further measurements under UV illumination at RT.

In order to demonstrate the power of aligned nanowires in contrast to the bundles of nanowires, we compared ZnO aligned nanowires prepared by LB technique with randomly aligned nanowires dropcast on the same chip, carrying out tests at RT with UV activation by 325 nm laser light.

Dropcast samples showed low current and noisy signal (Figure 6 (c)), along with some drift in the baseline: we observed current variations in some cases, but could not link the relative response to NO_2 concentration. Due to the random orientation of the NWs in dropcast sensors, their performance strongly depends on percolation through the interconnections between the NWs, a bottleneck parameter that significantly varies with preparation conditions. Furthermore, in percolating structures upon adsorption of oxidative molecules and blocking of some conducting branches, new random loops of various sizes are formed, which may lead to a low correlation between response and concentration. By contrast, the arrays of aligned NWs crucially minimize the issues arising from the intrinsically random nature of the dropcast nanowire network and percolations connected with the irregularity of the barriers at the random crossover junctions of the nanowire mats.

For aligned nanowire (Figure 6 (a)), conductivity follows the NO_2 concentration. The calibration curve (Figure 6 (b)) reports the mean value of relative response along with error bars, showing that a power law (a line in bilogarithmic plot) fits data as expected for metal oxide gas sensors. The lowest concentration tested was limited by the instrumentation available and is 1 ppm in the present case, but the results indicate that much lower values can be detected. We calculated that the limit for NO_2 detection is 0.2 ppm (see SI - Figure S4).

We studied the cross-interference of reducing gases in NO_2 detection in the optimal conditions for NO_2 sensing (RT + illumination at 325 nm). We chose H_2S as a reducing gas since it produces high response even at low concentration in ZnO [29]. Figure 6 **(**d) reports the current variation towards H_2S. No meaningful response signal was observed, probably due to RT operation.

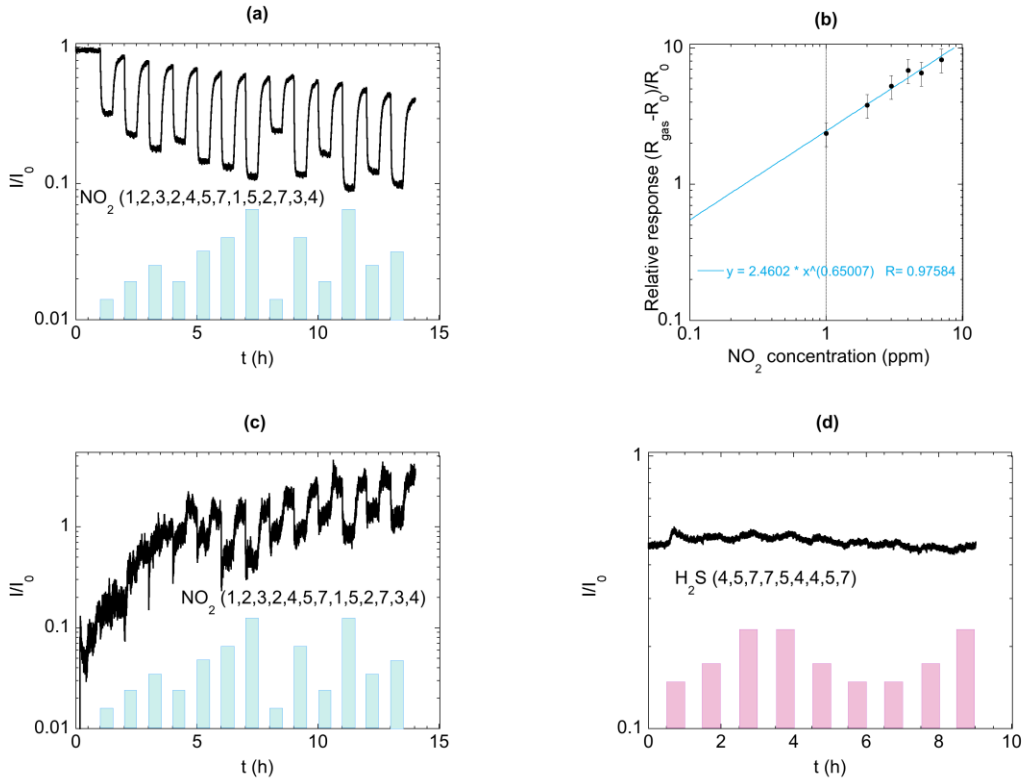

Figure 6: Comparison between the normalized current variation of aligned ZnO NWs (a) and dropcast NWs (c) for NO_2 detection. The measurement conditions were: RT, UV light activation and RH=30%. Gas pulses were random by purpose (1-2-3-2-4-5-7-1-5-2-7-3-4 ppm). (b) Calibration curves for NO_2 detection by LB aligned ZnO NWs reported in figure (a). (d) normalized current variation of aligned ZnO NWs towards H_2S.

UV illumination ensures an efficient way to obtain RT operation of our device. When NO_2 interacts with ZnO nanowires, the molecules chemisorb on the ZnO surface, forming a new acceptor state and thus decreasing the current. Due to band-to-band excitation, UV laser generates more electrons thus facilitating oxidative adsorption of NO_2, **Change 04** following the reaction [30]:

$$NO_{2(gas)} + e^- \rightarrow NO^-_{2(gas)} \quad \textit{(adsorption)} \qquad (1)$$

The increased density of photogenerated holes speed up the desorption rate of NO_2 gas molecules following the reaction:

$$NO_{2(gas)}^{-} + h^{+} \rightarrow NO_{2(gas)} \ (desorption) \qquad (2)$$

Improved photodesorption produces shorter response and recovery times of sensor working at RT with UV light (Figure 5 and Table 1), which become comparable to those of the sensor working at 200°C in the presence of blue light.

In the case of blue light excitation, the density of electrons excited from trap states is much smaller, as testified by the more modest current increase (Figure 4b), beside hole density is unaffected and response and recovery times much longer.

The too low operating temperature can explain the low cross-sensitivity to H_2S. When H_2S interacts with ZnO nanowires, the H_2S molecules react with preadsorbed oxygen species, thus acting as a reducing gas. The corresponding reaction is accompanied by releasing of electrons to the conduction band but requires an elevated temperature [31]. Holes generated by UV illumination at RT do not activate interaction of chemisorbed oxygen species with H_2S molecules on ZnO surface.

4. Conclusions

In summary, we have developed an easy and cost-effective way of separating and assembling the commercial metal-oxide nanowires on top of narrow-gapped electrodes based on the Langmuir-Blodgett technique. The obtained monolayers exhibit a high level of alignment (with orientation factors from 3 to 5) and reproducibility up to 80%. The used method is a promising

approach and can produce monolayers with an even higher alignment level provided that the uniform nanowires are being used.

The assembled nanowire arrays performed as a stable and sensitive photoactivated sensor to oxidizing gases, such as NO_2, with much higher sensitivity and lower noise in comparison with randomly oriented dropcast nanowires. We have shown that using UV illumination during the sensor operation guarantees measurable current, lowest noise, and fastest response compared to heating and blue light illumination.

Comparing the current decays after illumination of the sensors with different wavelengths allowed us to conclude that the trapping centers in the studied zinc oxide nanowires are located rather in the bulk region of the nanowires than on their surface.

The high reproducibility and sensitivity of the fabricated devices, as well as the versatility of the method, can make the LB-based approach a promising candidate for routine fabricating of high-performance gas sensors at a large scale.

Corresponding Author

Camilla.baratto@ino.it

ORCID: http://orcid.org/0000-0003-3130-363X

Author Contributions

The manuscript was written through contributions of all authors. All authors have given approval to the final version of the manuscript.

Acknowledgements

This work was supported by NATO SPS MYP project NANEOS, Grant No. 985043. V.G. thanks Project HPC-EUROPA3 (INFRAIA-2016-1-730897) for the support.

Supporting Informations

Scheme of the gold electrode chip used in the work with the insets showing two different configurations of the electrodes tested. Surface pressure isotherm taken during the assembling of ZnO nanowires monolayer. SEM image of the dropcast ZnO nanowires on top of the golden electrodes. Calculation of limit of detection for NO_2 sensing.

ABBREVIATIONS

RT: Room Temperature; LB: Langmuir-Blodgett; NWs: nanowires; FE-SEM: Field Emission Scanning Electron Microscope; RR: Relative Response.

REFERENCES

[1] H.Y. Huang, P.C. Xu, D. Zheng, C.Z. Chen, X.X. Li, Sulfuration-desulfuration reaction sensing effect of intrinsic ZnO nanowires for high-performance H_2S detection, J. Mater. Chem. A. 3 (2015) 6330–6339. https://doi.org/10.1039/c4ta05963h.

[2] O. Lupan, L. Chow, T. Pauporte, L.K. Ono, B.R. Cuenya, G. Chai, Highly sensitive and selective hydrogen single-nanowire nanosensor, Sensors and Actuators B-Chemical. 173 (2012) 772–780. https://doi.org/10.1016/j.snb.2012.07.111.

[3] C. Baratto, M. Ferroni, G. Faglia, G. Sberveglieri, Iron-doped indium oxide by modified RGTO deposition for ozone sensing, Sensors Actuators, B Chem. (2006). https://doi.org/10.1016/j.snb.2006.04.026.

[4] M. Epifani, N. Garcia-Castello, J.D. Prades, A. Cirera, T. Andreu, J. Arbiol, P. Siciliano, J.R. Morante, Suppression of the NO_2 interference by chromium addition in WO_3-based ammonia

sensors. Investigation of the structural properties and of the related sensing pathways, Sensors and Actuators B-Chemical. 187 (2013) 308–312. https://doi.org/10.1016/j.snb.2012.11.072.

[5] E. Comini, C. Baratto, G. Faglia, M. Ferroni, A. Vomiero, G. Sberveglieri, Quasi-one dimensional metal oxide semiconductors: Preparation, characterization and application as chemical sensors, Prog. Mater. Sci. (2009). https://doi.org/10.1016/j.pmatsci.2008.06.003.

[6] C. Baratto, M. Ferroni, G. Faglia, G. Sberveglieri, Iron-doped indium oxide by modified RGTO deposition for ozone sensing, Sensors Actuators, B Chem. (2006). https://doi.org/10.1016/j.snb.2006.04.026.

[7] J.D. Prades, R. Jimenez-Diaz, F. Hernandez-Ramirez, S. Barth, A. Cirera, A. Romano-Rodriguez, S. Mathur, J.R. Morante, Equivalence between thermal and room temperature UV light-modulated responses of gas sensors based on individual SnO_2 nanowires, Sensors and Actuators B-Chemical. 140 (2009) 337–341. https://doi.org/10.1016/j.snb.2009.04.070.

[8] W. Cheng, Y. Ju, P. Payamyar, D. Primc, J. Rao, C. Willa, D. Koziej, M. Niederberger, Large-area alignment of Tungsten oxide nanowires over flat and patterned substrates for room-temperature gas sensing, Angew. Chemie - Int. Ed. (2015). https://doi.org/10.1002/anie.201408617.

[9] O. Lupan, V. Cretu, V. Postica, M. Ahmadi, B.R. Cuenya, L. Chow, I. Tiginyanu, B. Viana, T. Pauporté, R. Adelung, Silver-doped zinc oxide single nanowire multifunctional nanosensor with a significant enhancement in response, Sensors Actuators, B Chem. (2016). https://doi.org/10.1016/j.snb.2015.10.002.

[10] F. Hernandez-Ramirez, A. Tarancon, O. Casals, J. Arbiol, A. Romano-Rodriguez, J.R. Morante, High response and stability in CO and humidity measures using a single SnO_2 nanowire, Sensors and Actuators B-Chemical. 121 (2007) 3–17. https://doi.org/10.1016/j.snb.2006.09.015.

[11] V. Demontis, M. Rocci, M. Donarelli, R. Maiti, V. Zannier, F. Beltram, L. Sorba, S. Roddaro, F. Rossella, C. Baratto, Conductometric Sensing with Individual InAs Nanowires, Sensors. 19 (2019) 15. https://doi.org/10.3390/s19132994.

[12] F. Shao, J.D. Fan, F. Hernandez-Ramirez, C. Fabrega, T. Andreu, A. Cabot, J.D. Prades, N. Lopez, F. Udrea, A. De Luca, S.Z. Ali, J.R. Morante, NH_3 sensing with self-assembled ZnO-nanowire μHP sensors in isothermal and temperature-pulsed mode, Sensors and Actuators B-Chemical. 226 (2016) 110–117. https://doi.org/10.1016/j.snb.2015.11.109.

[13] S. Jin, D.M. Whang, M.C. McAlpine, R.S. Friedman, Y. Wu, C.M. Lieber, Scalable interconnection and integration of nanowire devices without registration, Nano Lett. 4 (2004) 915–919. https://doi.org/10.1021/nl049659j.

[14] Y.B. Hahn, R. Ahmad, N. Tripathy, Chemical and biological sensors based on metal oxide nanostructures, Chem. Commun. 48 (2012) 10369–10385. https://doi.org/10.1039/c2cc34706g.

[15] C.L. Zhang, K.P. Lv, N.Y. Hu, L. Yu, X.F. Ren, S.L. Liu, S.H. Yu, Macroscopic-Scale Alignment of Ultralong Ag Nanowires in Polymer Nanofiber Mat and Their Hierarchical Structures by Magnetic-Field-Assisted Electrospinning, Small. 8 (2012) 2936–2940. https://doi.org/10.1002/smll.201201353..

[16] Y. Huang, X.F. Duan, Q.Q. Wei, C.M. Lieber, Directed assembly of one-dimensional nanostructures into functional networks, Science 80-. 291 (2001) 630–633. https://doi.org/10.1126/science.291.5504.630.

[17] J. Guilera, C. Fabrega, O. Casals, F. Hernandez-Ramirez, S. Wang, S. Mathur, F. Udrea, A. De Luca, S.Z. Ali, A. Romano-Rodriguez, J.D. Prades, J.R. Morante, Facile integration of ordered nanowires in functional devices, Sensors and Actuators B-Chemical. 221 (2015) 104–112. https://doi.org/10.1016/j.snb.2015.06.069.

[18] J.W. Liu, H.W. Liang, S.H. Yu, Macroscopic-scale assembled nanowire thin films and their functionalities, Chem. Rev. (2012). https://doi.org/10.1021/cr200347w.

[19] P. Yang, Wires on water, Nature. (2003). https://doi.org/10.1038/425243a..

[20] S. Acharya, J.P. Hill, K. Ariga, Soft langmuir-blodgett technique for hard nanomaterials, Adv. Mater. (2009). https://doi.org/10.1002/adma.200802648.

[21] L. Mai, Y. Gu, C. Han, B. Hu, W. Chen, P. Zhang, L. Xu, W. Guo, Y. Dai, Orientated langmuir-blodgett assembly of VO_2 nanowires, Nano Lett. (2009). https://doi.org/10.1021/n1803550k.

[22] K. Kartasalo, R.P. Polonen, M. Ojala, J. Rasku, J. Lekkala, K. Aalto-Setala, P. Kallio, CytoSpectre: a tool for spectral analysis of oriented structures on cellular and subcellular levels, BMC Bioinformatics. 16 (2015). https://doi.org/10.1186/s12859-015-0782-y.

[23] K.T. Chung, J.H. Reisner, E.R. Campbell, Charging phenomena in the scanning electron microscopy of conductor-insulator composites: A tool for composite structural analysis, J. Appl. Phys. 54 (1983) 6099–6112. https://doi.org/10.1063/1.331946.

[24] J.D. Prades, R. Jimenez-Diaz, F. Hernandez-Ramirez, S. Barth, A. Cirera, A. Romano-Rodriguez, S. Mathur, J.R. Morante, Equivalence between thermal and room temperature UV light-modulated responses of gas sensors based on individual SnO_2 nanowires, Sensors and Actuators B-Chemical. 140 (2009) 337–341. https://doi.org/10.1016/j.snb.2009.04.070..

[25] P. V Bakharev, D.N. McIlroy, Signal-to-Noise Enhancement of a Nanospring Redox-Based Sensor by Lock-in Amplification, Sensors. 15 (2015) 13110–13120. https://doi.org/10.3390/s150613110.

[26] M. Law, H. Kind, B. Messer, F. Kim, P. Yang, Photogenerated sensing of NO_2 with SnO_2 nanoribbon nanosensors at room temperature, Angew. Chem. Int. Ed 41 (2002) 2405-2408.

[27] V. Golovanov, V. Golovanova, T.T. Rantala, Thermal desorption of molecular oxygen from SnO_2 (110) surface: Insights from first-principles calculations, J. Phys. Chem. Solids. 89 (2016) 15–22. https://doi.org/10.1016/j.jpcs.2015.10.010..

[28] V. Golovanov, V. Smyntyna, G. Mattogno, S. Kaciulis, V. Lantto, Oxygen interaction with oxide gas sensors with different stoichiometric composition, Sensors and Actuators B-Chemical. 26 (1995) 108–112. https://doi.org/10.1016/0925-4005(94)01568-3.

[29] C. Baratto, Growth and properties of ZnO nanorods by RF-sputtering for detection of toxic gases, Rsc Adv. 8 (2018) 32038–32043. https://doi.org/10.1039/c8ra05357j.

[30] Y. Sahin, S. Ozturk, N. Kilinc, A. Kosemen, M. Erkovan, Z.Z. Ozturk, Electrical conduction and NO_2 gas sensing properties of ZnO nanorods. Applied Surface Science 303 (2014), 90-96.

[31] J. Kim, K. Yong, Mechanism study of ZnO nanorod-bundle sensors for H_2S gas sensing, J. Phys. Chem. C. 115 (2011), 7218-7224, https://doi.org/10.1021/jp110129f.